Chapter 3

Robotic organism description

"Science is not only a disciple of reason but also one of romance and passion."

Stephen Hawking

This doctoral thesis uses leg modules designed previously from the ROMERIN robot. In this dissertation, a robotic organism is proposed consisting of N leg modules and a central body where the modules are housed. Although the process to achieve a functional leg module has gone through many iterations, the main three prototypes are described in this chapter. The first prototype was previously designed and is described in detail, whereas for the second and third prototypes, only the changes undergone are described.

3.1 Terminology

In the search for a robotic system capable of performing different inspection and maintenance tasks, all leads to the need for a modular, versatile, and adaptable robot. For a modular legged and climbing (L&C) robot, a leg is considered a single module that is attached to a body, which is the part of the system to be controlled. In fact, each module is one of the parts of a modular robot that has sensorization, actuation, and processing capabilities, that is, it has sensors to detect the environment and its own state, actuators to act over the exterior world, and a processing area to communicate with other devices and control sensors and actuators. According to these premises, each module has all the required components and features of a robot, and it may consider so. To avoid confusions, along this dissertation, the words leg, module, or leg module are commonly used in the same way, and they are not denoted as robots. The concepts of robot or modular robot appear as the definition of the whole system. Because modules could be considered as robot by themselves, the word organism or robotic organism appears as a definition of the entire modular robot. Then, an organism is understood as a coordinated combination of modular units, that is, a living system that functions as an individual entity.

In summary, the following terminology is used:

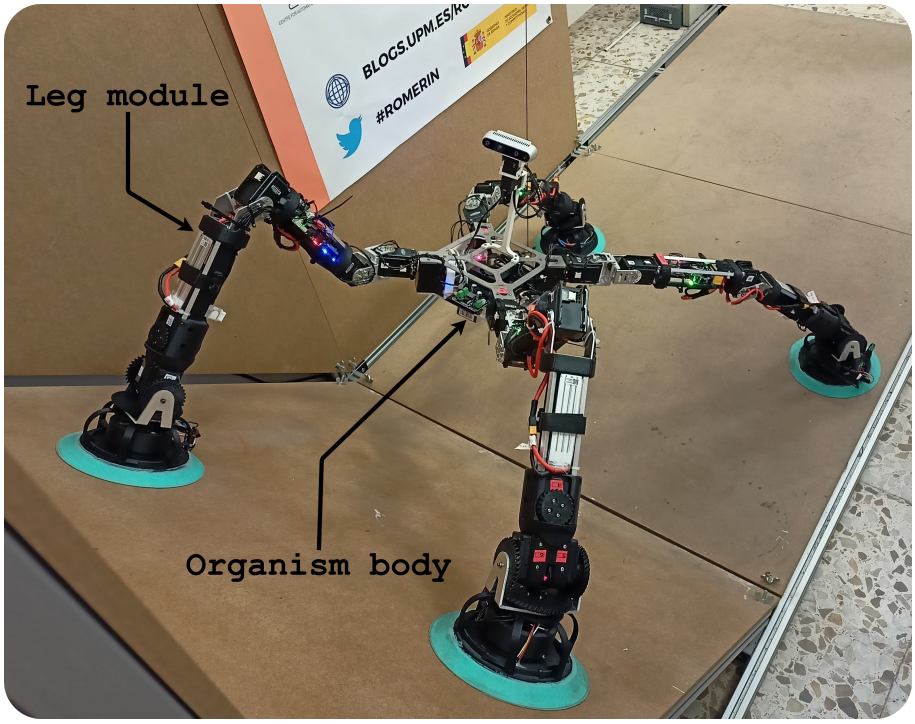

Figure 3.1: ROMERIN robotic organism components.

- **Module**. A module is a component of a set of parts that performs, totally or partially, typical tasks of a robot and that has the ability to interact with other modules. In the case of ROMERIN, a module is a component with sensorization, actuation (motion and adhesion system), processing, and communication capabilities. In this case, the terms leg module, leg, and module are used indistinctly.

- **Body**. System that includes the necessary components for processing, coordination, and communication of modules, and perception of the environment. In the case of ROMERIN, the terms body and organism body are used indistinctly.

- **Robotic organism**. Set of modules and other components that perform a function as a set. In the case of ROMERIN, a robotic organism is a set of modules and body that combine the abilities of all of them to walk and climb in the environment according to the user premises. In this case, the terms robotic organism and robot are used indistinctly.

3.2 Modularity concept

The concept of ROMERIN as a fully modular climbing robot is based on the design and development of a leg that is, by itself, a complete and autonomous robot but has the ability to share energy with the rest of the legs. The adhesion system, which is described later in this chapter, is based on the placement of an active suction cup at the end of each of its legs.

Each of the legs is equipped with the following elements:

- A dedicated microcontroller for control.
- Specific electronic devices for robot instrumentation. The leg can properly distribute the energy to the different components and other modules.
- A battery that allows it to operate autonomously.
- A completely self-contained actuation system. A module has all the needed to move. Under nominal conditions, it does not require an external power supply.
- Communication with other modules and outside.
- A sensorized suction cup with a vacuum turbine to adhere the leg to the surface.

Therefore, the robotic leg module is a robot by itself. It is a completely autonomous basic unit. It is able to move and manage its own resources. However, it is also prepared to collaborate with other robotic leg modules. Through the communication system, it can handle requests from outside and also coordinate its actions to be able to walk or climb with the help of other modules. Its design is capable of contributing to the mechanical task of the whole and, if necessary, even providing the energy required for it.

3.3 First version of the leg module

The first version of the leg module was first introduced in [Brito, 2020], and was formally defined in [Hernando et al., 2022]. It was designed as an articulated leg to gather the advantages of high maneuverability and flexibility (Table 2.2).

3.3.1 Mechanical design

The first version of the robotic module has been designed with 7 degrees of freedom (see Figure 3.2) disposed as follows:

- 3 actuated rotational joints in the shoulder (q1, q2 and q3), formed by three power servomotors.
- 1 actuated rotational joint in the elbow (q4), formed by one power servomotor.
- 3 actuated rotational joints in the wrist (q5, q6, and q7), formed by three servomotors for wrist orientation.

The typical structure of most agile walking robots is a kinematic configuration of 4 DOF. To this configuration, 3 DOF has been added to orient the suction cup located at its end against an external plane.

Due to their compact and smart actuator characteristics, the Dynamixel servomotors were chosen. Dynamixel servomotors provide feedback of position, velocity, intensity, etc. The module uses an 8.4Nm maximum stall torque servo (MX-106T) in the first joint and 6.4Nm servos (MX-64) in the second, third, and fourth. However, on the wrist, it is desirable to maintain a certain degree of reversibility, and it is not necessary to exert excessive torque. For this reason, three servos with 0.39Nm of stall torque (XL-320),

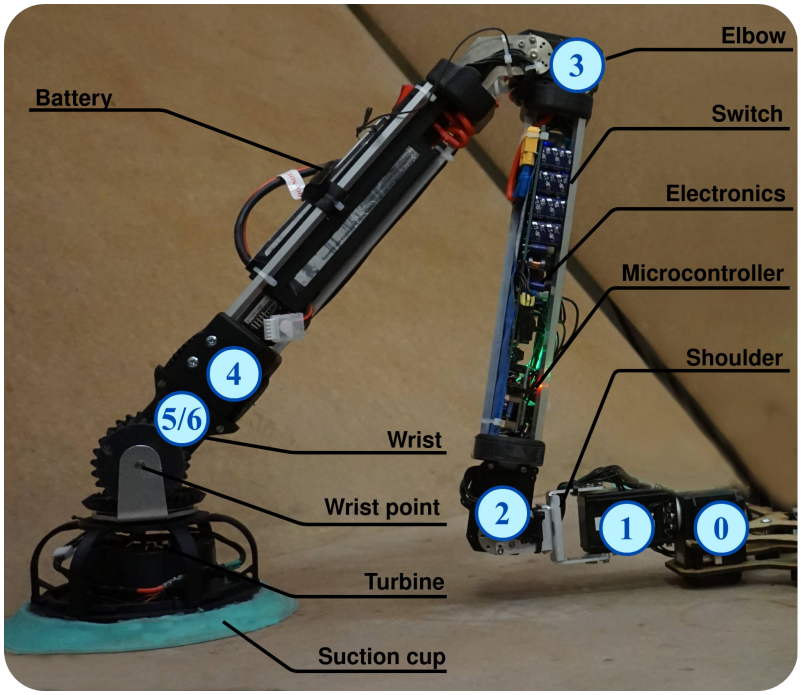

Figure 3.2: First version of the ROMERIN leg module.

whose axes are arranged concurrently, have been installed on the wrist with a differential configuration of the last two axes, analogously to the wrists of most industrial robots. The weights of the parts and components and joint ranges are shown in Table 3.1. It is worth mentioning that the ranges in the last two joints are indicated from a kinematics point of view, that is, taking into account the combination of movements of the two actuators mounted in a differential configuration.

Part	**Weight (g)**	**Link**	**Weight (g)**	**Joint**	**Range (°)**
Shoulder	554	1	185	1	[-180, 180]
		2	148	2	[-110, 110]
		3	221	3	[-110, 110]
Arm	572	4	572	4	[-35, 170]
Forearm	785	5	785	5	[-180, 180]
Wrist and suction cup	519	6	107	6	[-90, 90]
		7	412	7	[-180, 180]
Total weight	**2430**				

Table 3.1: Parts weight and range of the first version of the module.

The total module length with the suction cup is 987 mm. The distance between the shoulder and the elbow is 332 mm, and the distance between the elbow and the wrist is 383 mm. The link corresponding to the forearm has the battery inside, while the other link is reserved for carrying control and power electronics. In this way, the weight is distributed with the heaviest component as close as possible to the attachment point.

Although this initial design was intended to have the heaviest components close to the attachment point in order to reduce torques during the module stance phase, it has

the drawback that the torque requirements are higher when the module is in swing phase (moving the leg from one place to another).

3.3.2 Suction cup

The suction cup has different objectives: a) provide a flexible sealing zone with which to generate a vacuum chamber, avoiding pressure losses as much as possible; b) generate enough friction to prevent slippage between the contact surface and the suction cup, so that the robot can continue climbing while enough vacuum is generated to remain fully attached; and c) achieve a steady state of negative pressure.

For sticking to walls or ceilings, each of the robotic modular legs is equipped with a sensorized suction cup placed at its end. To create the needed vacuum, every suction cup includes its own centrifugal impeller and motor. This configuration has the main advantage of better adhesion capacity in the presence of cracks or defects or on rough surfaces. The fact that suction is generated independently in each leg avoids the effect of pressure loss in the entire robot when one of the suction cups is placed in an area with excessive air loss. The design and construction process of the suction cup has been optimized by developing a CFD (computer fluid dynamics) modeling to determine the best performing configuration to achieve a power consumption as low as possible while maintaining acceptable vacuum values [Hernando et al., 2021b]. Therefore, the rotational speed can be limited to reduce the electrical power needed. The modeling and optimization procedure has been done using two prototypes: a test bench prototype and an onboard robot prototype. The design of the suction system for both prototypes consists of a housing, impeller (with integrated motor), motor cover, coupling to the robot leg and suction cup, as shown in Figures 3.3(a) and 3.3(b).

Analytical and numerical models were developed to predict the behavior of the system for different configurations. Models were validated, using measurement of test rig, by calibrating an arbitrarily defined inlet height that simulates the leakage flow. Then, different geometric parameters were varied to determine the best performing configuration based on the vacuum/power consumption ratio value. Finally, the model was used to optimize system parameters, such as the number of impeller blades.

The suction system is equipped with three proximity sensors (STMicroelectronics VL6180X, illustrated in Figure 3.3(b) with red circles) capable of measuring the distance to the nearest object using Time-of-Flight technology, and a digital pressure sensor (Bosch BMP180, illustrated with a green circle) to measure the pressure exerted and the temperature. The last sensor lets the system react to flow losses that lead to pressure drops, increasing the speed of the turbine to compensate.

The components of the suction cup, illustrated in Figure 3.4, are:

1. Silicone suction cup. It is composed by:
    - a rigid structure, where sensors are mounted, where the entire suction cup attaches to the leg, and where the silicone part attaches,
    - the silicon part, which prevents low-pressure air from escaping from the suction cup.
2. Stator: Fixed part in which the rotor will rotate.

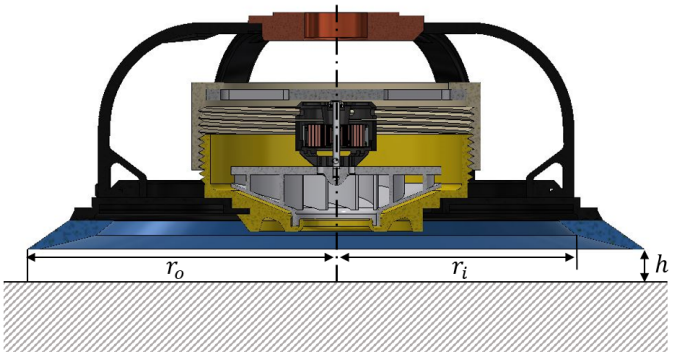

(a) Model of the suction cup.

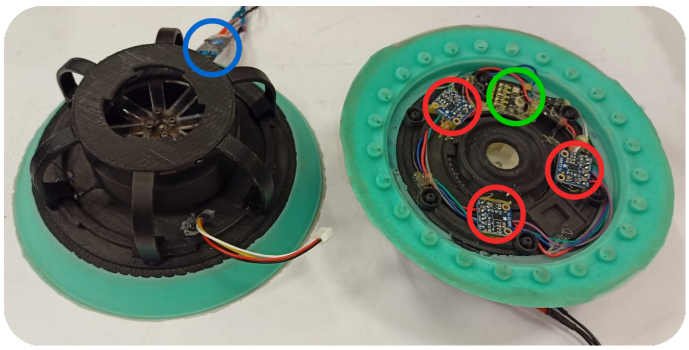

(b) Real view of the suction cup. Proximity sensors (VL6180X) are rounded in red, while the pressure sensor (BMP180) is rounded in green. The motor driver is highlighted with a blue circle.

Figure 3.3: Suction system.

3. Stator cover: Upper part of the stator that holds it by screwing it. It includes a methacrylate piece that holds the rotor while it remains fixed during its rotation

4. Motor with turbine and clamping part: Rotating part that sucks air from the suction cup to generate vacuum.

5. Separator ring: Piece that adjusts the distance between the rotor and the stator.

6. Hitches: Flexible system that eliminates torsion and efforts to the suction cup.

In this version, the "Mold Star 15 Slow" mixture was used, it is a platinum-based silicone with a bluish color. The advantages are its flexibility and the friction that can be acquired. However, the silicon part of this suction cup easily disassembles during robot operation, which means an instantaneous loss of pressure and causes the robot to fall.

Since the objective of the thesis consists mainly in the control of the robot, it is necessary to study the duration of the battery in different situations, as well as the physical limits that must be taken into account in the climbing process. For this reason, a series of experimental tests have been carried out within the framework of the thesis. Thus, Table 3.2 shows a study of the current consumption of a module and the vacuum pressure of the suction cup in different situations to support its own weight when that module is

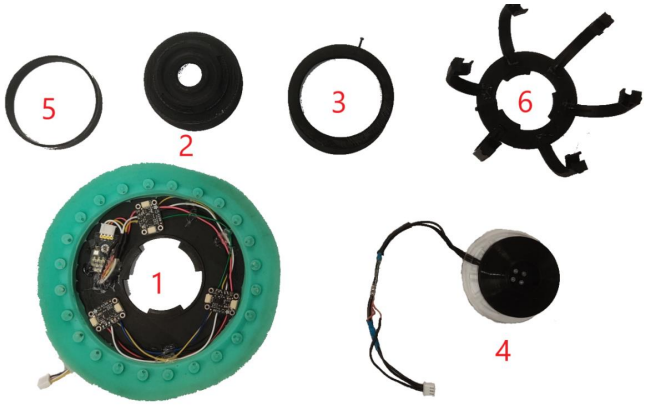

Figure 3.4: Components of the first version of the suction cup. Source: [Valero, 2021]

upright. During these tests, the robot blocks the first four motors in the zero position, whereas the last three motors are passive to avoid overcurrents. The majority of the current is consumed by the suction cup motor, while a small portion is used to keep the motors in the desired position. Table 3.2 indicates the material in which the suction cup is attached (Figure 3.5), its porosity, the wall slope, the consumption of vacuum current (while the module is attached), the absolute pressure found within the suction cup (denoted as vacuum pressure), the speed of the suction cup turbine and the battery duration under the given conditions.

The differences in the results for different materials are mainly due to the porosity and roughness of the material. A greater pressure drop is produced with higher porosity values. Porous materials need more turbine speed to generate the same vacuum pressure in the suction cup, being the maximum turbine speed of 25000 rpm. As a consequence, power consumption increases and battery duration decreases. This should be taken into account during the task plan, since robot autonomy is affected by the material in which the robot works.

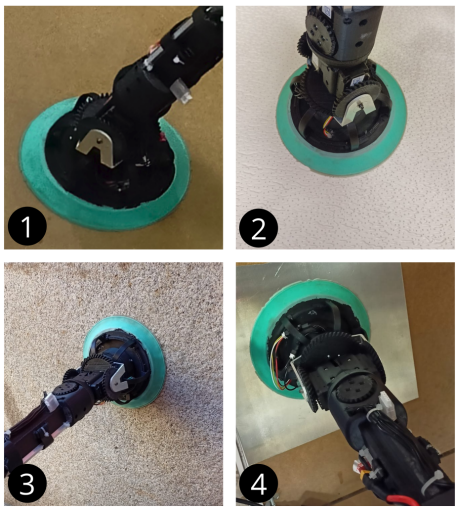

Figure 3.5: Suction cup attached to different materials. 1. Wood veneer. 2. Plaster. 3. Concrete. 4. Steel.

As expected, the motor consumes considerably more power when the suction cup does

Material	Angle (°)	Current (A)	Relative pressure (Pa)	Power throttle (%)	Battery duration (min)
Wood veneer (low porosity)	0	1.45	1791	40	153
	45	2.64	3678	70	82
	90	3.08	4190	90	71
	135	2.75	4145	75	79
	180	1.7	1975	50	129
Plaster (high porosity)	0	1.67	1856	45	131
	45	2.85	3740	70	77
	90	3.26	4250	100	67
	135	2.91	3620	70	76
	180	2.12	2084	55	104
Concrete (very high porosity)	0	1.75	1801	50	127
	45	3.09	3705	80	72
	90	3.44	4120	100	64
	135	3.12	3722	80	71
	180	2.35	2105	65	94
Steel (low porosity)	0	1.54	2012	45	144
	45	2.74	3650	75	81
	90	3.15	4078	100	70
	135	2.94	4221	80	76
	180	1.75	1921	50	127

Table 3.2: Results of the robot test when the suction cup is attached to different materials and the module is upright. The results are relative to the limit at which the suction cup is released. Relative pressure represents the negative increase of pressure below atmospheric pressure.

not adhere. This is because the air is denser and therefore the turbine requires more power to achieve the same rotational speed. The duration of the battery also changes, and it must be taken into account in order to calculate the autonomy that the robot will have depending on the task to be carried out.

Figure 3.6(a) shows a comparison of the limit point at which the arm detaches from the surface in different materials and inclinations. Similarly, in Figure 3.6(b), a comparison of the battery duration for different materials and the adhesion inclination is shown. The most problematic material is concrete due to its porosity. On the other hand, plaster, which is a porous material, performs well on sloping and vertical walls due to its high roughness.

3.3.3 Electronics

The electronic board embedded in the robot has several functionalities (Figure 3.7). Module control is carried out using the ESP32-DevKitC V4 microcontroller, which includes an ESP32-WROOM-32. This provides a controller with the necessary ports to control the hardware, as well as many communication channels with the outside. In addition to sev-

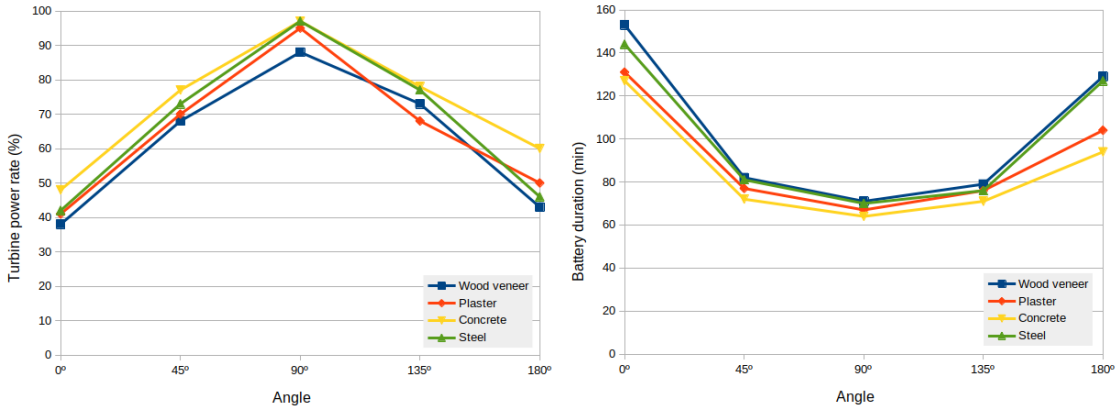

(a) Limit point of the turbine power rate at which the arm detaches in different inclinations.

(b) Battery duration of a module when operating on different inclinations.

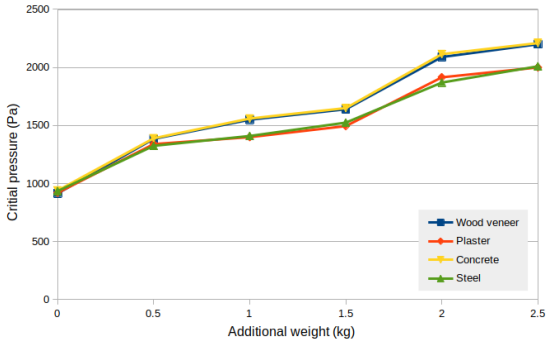

(c) Critical detaching pressure with different weights.

Figure 3.6: Analysis of first version of suction cup with different materials.

eral UARTs, it includes the capability to communicate via CAN, I2C, I2S, ISP, Bluetooth, and Wi-Fi. Since the microcontroller works at the logic level, electronics are required to adapt the communication to the physical level. In our case, it is necessary to do it for the UART (TTL & RS485) and the CAN bus. The first is used to communicate with the motors, while the latter is intended to be used to communicate with the outside. The CAN bus allows us to easily add and remove elements from the system. The board also includes a set of very useful LEDs to reflect the status.

However, the most complex part of electronics is the power part because of the ability to share energy.

With the idea of making the energy sharing system as adaptable and resilient as possible, the power electronics have been designed with the following functionalities:

- Two bidirectional protection modules against reverse polarity and overvoltages. One is located at the battery input, and the other at the connection to the power bus.
- Short-circuit protection circuit to protect the step-down DC/DC converters that supply the motors.
- A voltage level adaptation stage.

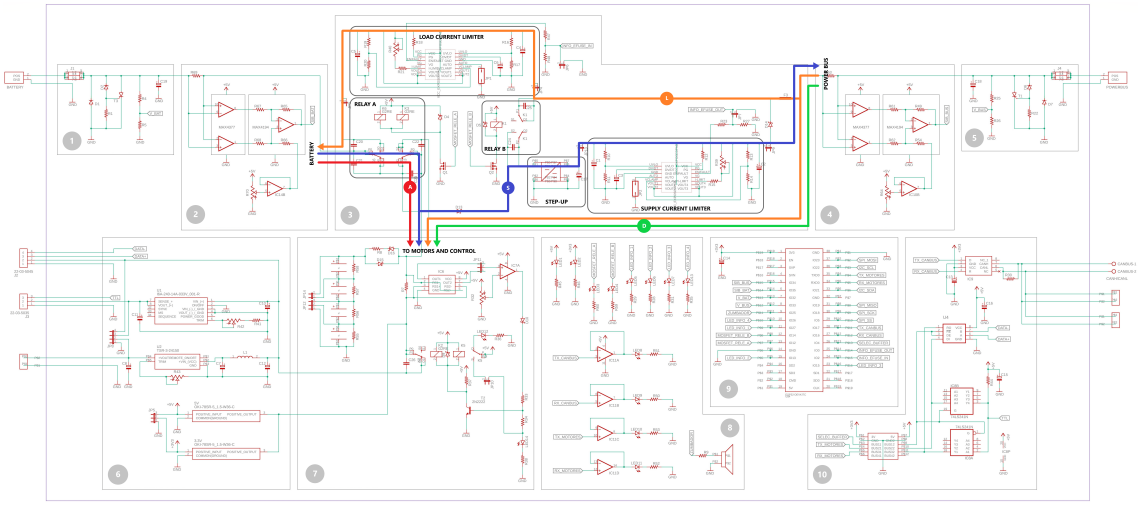

Figure 3.7: Schemmatic diagram of the electronics control board. (1) Battery bidirectional protection against reverse polarity and over-voltages. (2) Bidirectional battery current sensor . (3) Power sharing electronics. (4) Bidirectional power bus current sensor . (5) Power bus bidirectional protection against reverse polarity and over-voltages. (6) Step-down DC/DC converters . (7) Short-Circuit protection circuit. (8) Test leds. (9) Microcontroller. (10) Communications HW. (For interpretation of the components of the figure, the reader is referred to the web version of [Hernando et al., 2022].)

- Two bidirectional current sensors at the input of the battery as in the connection to the power bus.

- A circuit that manages the energy operating modes of the leg. This circuit includes supercapacitors that allow safe switching between different operating modes.

Bidirectional current sensors have been made by combining two differential instrumentation amplifiers (see Section 4 in Figure 3.7). Their input terminals are cross-connected to a shunt resistor. In this way, when the current goes in one direction, the output of one amplifier is proportional to the current, whereas the output of the other is null. When the current flows in the opposite direction, the roles of both amplifiers are reversed. These two signals enter an instrumentation adder/subtractor amplifier that includes an offset. Setting the offset to 2.5V, the signal from the first amplifier to the positive input, and the signal from the second amplifier to the negative, we will have a linear bidirectional measure of intensity in the range of 0-5V. When the output voltage is the same as the offset voltage, the running intensity is zero. In this way, because negative voltages are not used, there is a signal that can be easily interpreted by the microcontroller.

To summarize, the electronic board is responsible for controlling the motors of the module, as well as reading the status of the motors from the embedded microcontroller of the motors. In addition, it controls the actuation of the suction cup and the reading of its sensors. Finally, it periodically sends the status of the entire module to the high-level controller and receives the commands to be executed.

3.3.4 Energy sharing

A power bus with a voltage higher than that required for its operation is used to share energy between the different modules. Since protective elements result in a decrease of 1.6V, the bus voltage has been set to 18V so that an effective 16.4V will reach the module and the battery (LiPo 4S 3700 mAh, 45C).

Each module has the electronics required to import or export energy from the bus. Energy will be exported through a step-up converter capable of raising the variable battery voltage to the constant 18V bus voltage. This circuit includes an electronic fuse that limits the energy delivered. When the energy from the bus is used, the module will be responsible for adapting the voltage levels to those required by its different components.

The four power-sharing operation modes described above are obtained by the logic of two DPDT relays (Double Pole Double Throw). The way in which these modes are achieved is explained below.

The components and current flow through the power sharing electronics are also shown in Figure 3.7 identified with different colors and the corresponding letters. It is a schematic representation that reflects why elements circulate the intensity according to the active mode, as explained below.

- Autonomous mode (A): The module's battery powers only its electronics and actuators. The energy only passes through relay A. In this way, the rest of the circuit (i.e. the current limiters to the outside and the step-up converter stage) is not powered, and the power bus is not connected to the module.
- Supply mode (S): The battery powers the module electronics and its motors through relay A. In addition, relay B is activated, so the current passes through an electronic fuse that limits the current to the step-up, which raises the voltage to match the power bus voltage. The current limitation of the battery is disconnected.
- Loading mode (L): As relay A is activated, the power bus supplies both the module and the battery. In the second case, the current passes through another electronic fuse that limits the charging speed. The step-up converter stage is disconnected because relay B is not active.
- Damaged mode (D): This mode is specifically designed to take into account the case of a damaged battery. Relay A isolates the module from it, while the second relay directs the power bus exclusively to the module, leaving the battery disconnected.

By default, the modules operate in autonomous mode. In general, each module is considered to have the necessary power for its operation.

3.4 Second version of the leg module

After several experiments, it was considered to reduce the size of the leg and make the robot stronger. It implies a size reduction of the electronic board, and, consequently, some detected errors in the previous version were corrected. The need to strengthen the leg is because the chosen coreless Dynamixel motors cannot maintain the maximum indicated stall torque for a long time, and the design of the first version selected the motors by the

stall torque. Furthermore, the nominal torque cannot exceed 20% of the maximum stall torque, and it was not feasible with the actuators chosen in the first version. The new version also improves the suction cup by integrating the electronics and improving the manufacturing system.

3.4.1 Mechanical design modifications

Computing the static model, it has been revealed that the motors were too weak in terms of power, so a shorter and lighter mechanical design is required. Thus, the second version of the leg modules is created as shown in Figure 3.8. As a result, the length with the suction cup has been reduced from 987mm to 761mm, and the weight was curtailed from 2.43kg to 2.08kg.

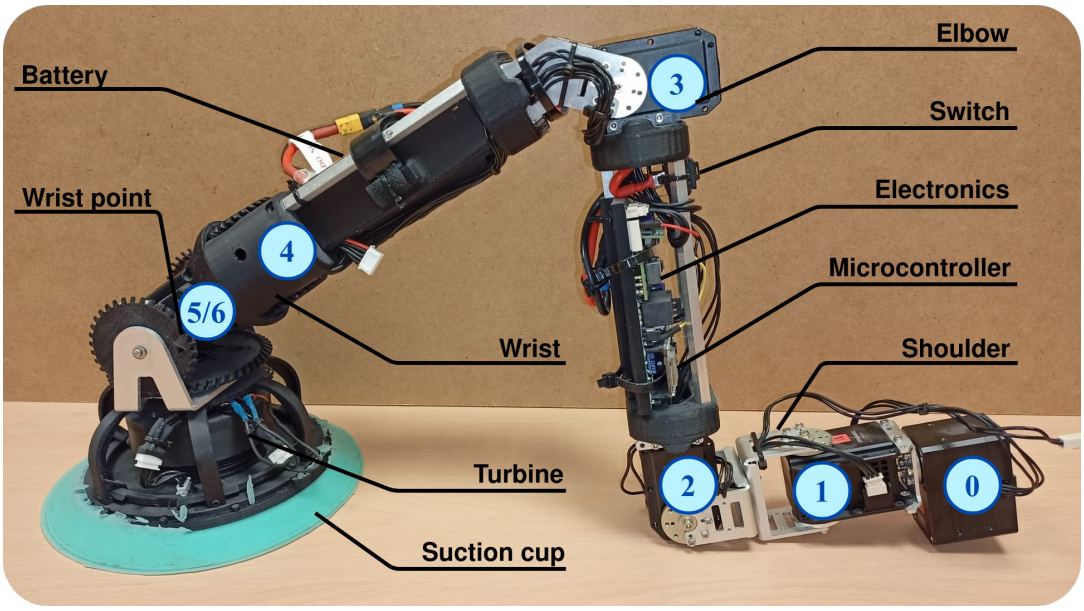

Figure 3.8: Second version of the ROMERIN robotic leg.

This module version uses a 9.9 Nm stall torque servo (XH540-W270-T) in the first joint and 6.4 Nm servos (MX-64) in second, third and fourth. The fourth servo performance was improved by changing the inner motor[1]. The last three models of servos and their configuration were maintained in the wrist. The weights of the parts and components are shown in Table 3.3.

3.4.2 Suction cup modifications

In order to improve robustness and ease of assembly, this version includes a circular electronic board, named the circular crown, that integrates the suction cup sensors [Valero, 2021]. This version of suction system is equipped with the same proximity sensors (STMicroelectronics VL6180X), and a different digital pressure sensor (BMP180), which is a high precision, tiny pressure sensor module that measures the pressure exerted and the temperature. The turbine motor driver keeps out of the electronic board in this version.

[1]Hack a servo: `https://blogs.upm.es/romerin/2022/03/10/hacking-of-dynamixel-motors/`

Part	Weight (g)	Link	Weight (g)	Joint	Range (°)
Shoulder	545	1	185	1	[-180, 180]
		2	148	2	[-110, 110]
		3	212	3	[-110, 110]
Arm	389	4	389	4	[-55, 160]
Forearm	627	5	627	5	[-180, 180]
Wrist and suction cup	519	6	107	6	[-90, 90]
		7	412	7	[-180, 180]
Total weight	**2080**				

Table 3.3: Parts weight and range of the second version of the module.

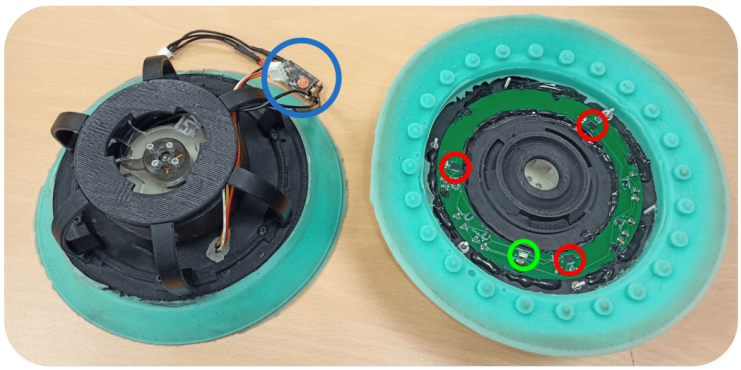

Figure 3.9: Real view of the second version of the suction cup. Proximity sensors (VL6180X) are rounded in red, the pressure sensor (MS5611) is rounded in green, and the motor driver is rounded in blue.

Consumption of suction cups under different circumstances does not vary substantially compared to the first version of the suction cup.

3.4.3 Electronics modifications

With the aim of reducing the size, the electronic board was redesigned to be smaller and more compact that could still be used to control the robot [Figueroa, 2021]. This new design split the previous board into two different ones:

- Electronic control board. It includes all the indispensable tasks of the previous board, such as the control of the servos, communication with a master computer, and the control of the suction cup. The size of this electronic board is considerably reduced to reduce arm length (Figure 3.10).
- Energy sharing board. It includes the energy sharing features between modules, as explained in Section 3.3.3. This version of the board (Figure 3.10) is located over the control electric board, consequently reducing the length of the arm. It still has four defined modes (Figure 3.11: autonomous mode (A), supply mode (S), loading mode (L) and damage mode (D).

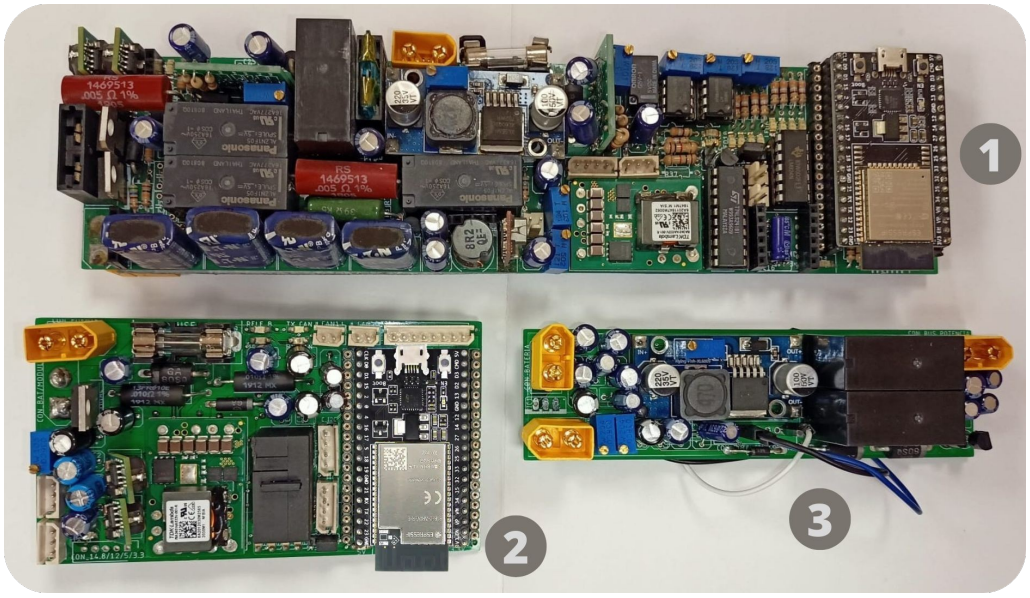

Figure 3.10: Comparison between the first and second version of the electronic board. (1) First version of the electronic board with energy sharing capabilities, (2) second version of the electronic board, and (3) second version of the energy sharing board.

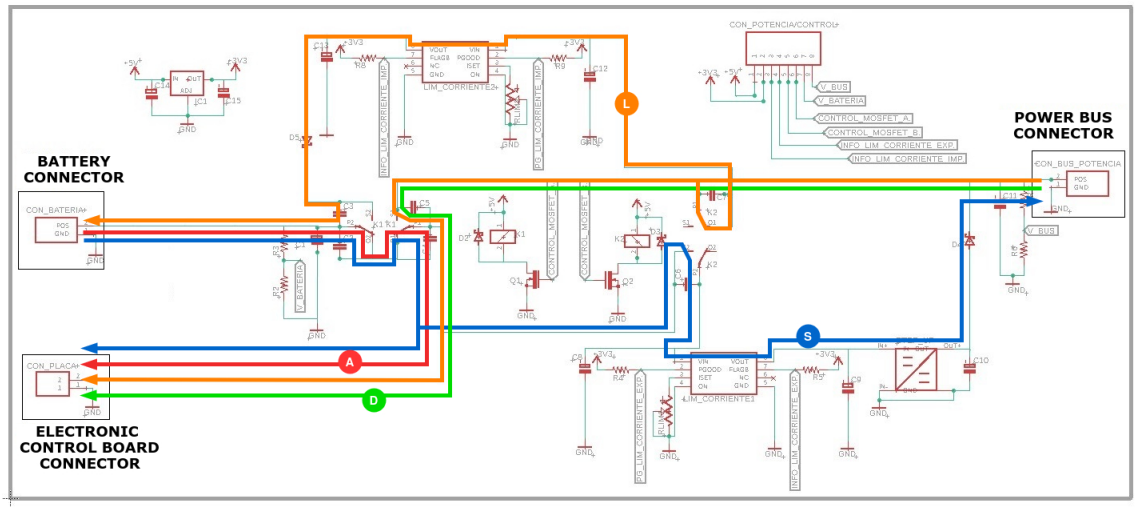

Figure 3.11: Energy sharing electronic board circuit. This figure has been modified from the original found in [Figueroa, 2021].

3.5 Third version of the leg module

3.5.1 Mechanical design modifications

The modules size has again been reduced for the following reasons:

- The first motor was supporting a strong radial force.
- Due to the radial force, the first motor shaft was buckling, and, consequently, the

gaps and inaccuracies increase considerably.

- The static model computation still reveals that the motors are weak in terms of power, so a shorter and lighter mechanical design is more recommendable.

As a result (see Figure 3.12), the length, with the suction cup included, has been reduced from 761mm to 711mm, and the weight was curtailed from 2.08kg to 1.94kg, which is broken down in Table 3.4.

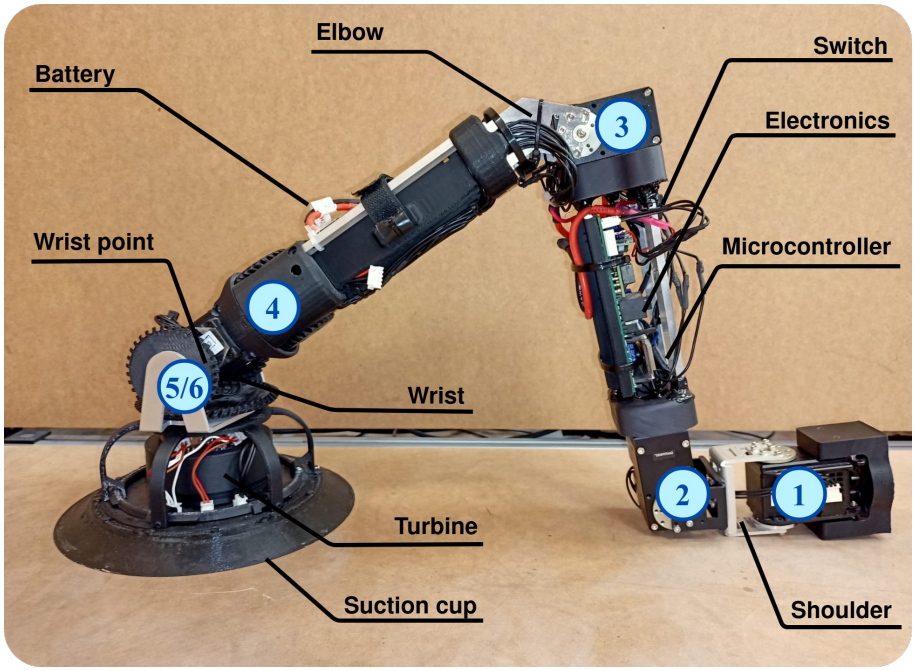

Figure 3.12: Third version of the ROMERIN robotic leg.

Part	Weight (g)	Link	Weight (g)	Joint	Range (°)
Shoulder	394	1	182	1	[-110, 110]
		2	212	2	[-115, 104]
Arm	443	3	443	3	[-55, 160]
Forearm	627	4	627	4	[-180, 180]
Wrist and suction cup	479	5	107	5	[-90, 90]
		6	372	6	[-180, 180]
Total weight	**1943**				

Table 3.4: Parts weight and range of the third version of the module.

3.5.2 Suction cup modifications

The previous version of the suction cup had the following drawbacks:

- The methacrylate piece vibrates too much and its use generated cracks that could cause it to burst, endangering the rest of the components.

- The silicone on the suction cup separates very easily. This makes climbing very difficult and dangerous.

- The molding process is cumbersome and requires the use of silicone to prevent leakage. It is very common for suction cups to break during unmolding due to carelessness.

- Electronics were manually glued to the rigid structure of the suction cup. It is desired to have an all-integrated system.

To start with, the design of some pieces, such as the hitches and the methacrylate pieces, has been improved (Figure 3.13) after an effort analysis [Valero, 2021].

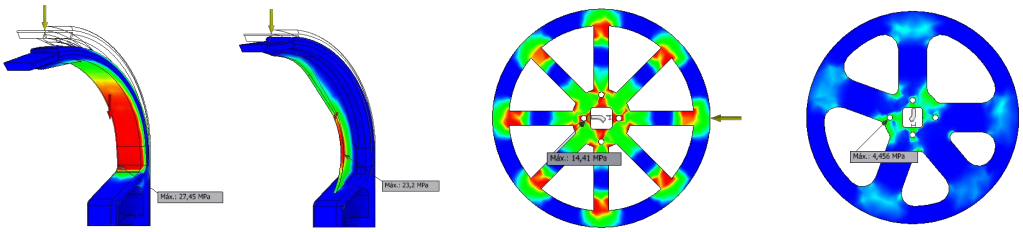

(a) First version of the hitches. (b) New version of the hitches. (c) First version of the methacrylate piece. (d) New version of the methacrylate piece.

Figure 3.13: Design improvements of the hitches and methacrylate piece. Source: [Valero, 2021].

Furthermore, in this version, the suction cup can be fully printed in plastic using 3D printers. The most substantial change is found in the largest part of the suction cup, which is made up of a rigid plastic part and a flexible plastic part (printed with Filaflex TPE 82A). Both are printed at the same time with two different materials in such a way that they are fully attached and cannot be separated without breaking the suction cup.

To increase the friction between the suction cup and the environment, it was decided to apply the product "Polygel 35", a mixture of platinum rubber, which in liquid format can be spread on any surface and remain highly adhered. Being a rubber, its coefficients of friction are much higher than those of the flexible filament, equaling that of silicone. The application format is about mixing two materials in equal quantities, which produces an exothermic reaction that activates the rubber, forming a thick blue liquid, which can be applied over the flexible plastic. When spreading a layer of this material and letting it mature for 16 hours, a flexible filament suction cup is achieved with better performance than the previous model and without the use of molds. This new version of the suction cup has the drawback of degradation, which occurs due to dirt and causes the friction of the glue to drop, so it requires maintenance and periodic application.

Figure 3.14 shows the third version of the suction cup, in which the new electronic circular crown is observed. In this version, the electronic board includes the turbine motor driver, achieving a more compact, easy-to-mount, and robust system [Valero, 2021].

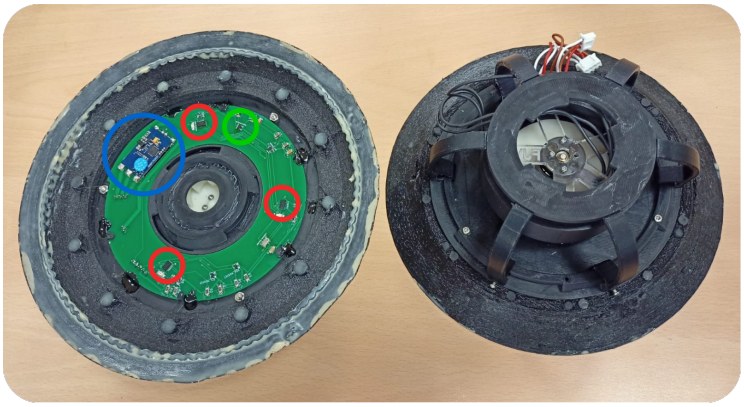

Figure 3.14: Real view of the third version of the suction cup. Proximity sensors (VL6180X) are rounded in red, the pressure sensor (MS5611) is rounded in green, and the motor driver is rounded in blue.

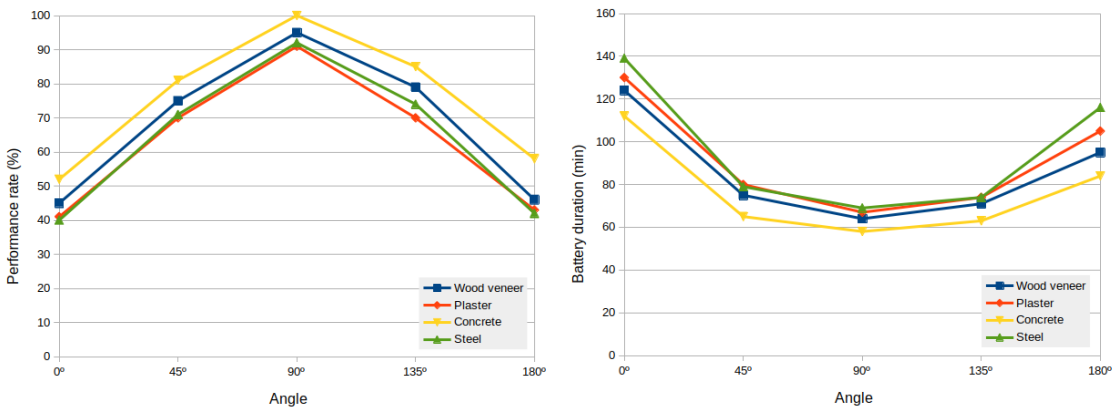

(a) Limit point of performance rate at which the arm detaches in different inclinations.

(b) Battery duration of a module when operating on different inclinations.

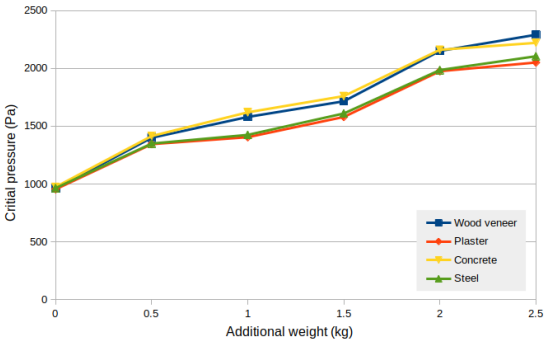

(c) Critical pressure of detaching with different weights.

Figure 3.15: Analysis of second version of suction cup with different materials.

3.6 Leg module overview and communication

Based on the idea of reducing complexity, modularizing, and releasing workload from the central controller (CC), we propose a 7 DOF robotic module [Hernando et al., 2022] that evolves to a 6 DOF module and serves as a tool for a whole organism to walk and climb. It is important to point out that the first mechanical iteration of the module was designed to have more than 6 DOF in such a way that it allows the module to select the most suitable and safer configuration, optimizing the torque that appears at critical joints. Thus, the module was made up of seven servomotors, where the first one is considered a state variable and serves to facilitate the change of plane. However, since although the most powerful servomotors of Dynamixel were unable to support the static forces that appear during operation, the number of joints, the length, and weight have been reduced to guarantee safer and proper performance. The motors are grouped into three groups, the shoulder (joints 0, 1), the elbow (joint 2) and the wrist (joints 3, 4, and 5). The axes of the last three joints (wrist) are arranged concurrently, with the last two axes in a differential configuration. As a result of that, similar to what happens in most industrial robots, the last three axes intersect at the same point (called wrist point) in such a way that whenever the gripping system is grabbed to a surface, the wrist point stays static. Unlike ball joints where the wrist is not actuated, such as the ROMHEX robot approach [Hernando et al., 2021a], the concurrently actuated, reversible, and differential approach of the wrist allows the module to focus its suction cup against the surface of contact during the swing phase of the walking and climbing gait; that is, this configuration allows orienting the plane and rotation of the suction cup to place it in the optimal gripping conditions. During the stance phase, the wrist motors are turned off to allow a free position of the suction cup in such a way that the wrist behaves as a ball joint.

Due to the morphology of the wrist, the motion of the last two motors does not correspond directly to the motion of the joints. Positive movement of the fifth joint is achieved with coordinated movement in the opposite direction of motors 5 and 6, rotating motor 5 in the positive direction. On the contrary, the positive movement of the sixth joint is achieved with coordinated movement and in the same direction of both motors, rotating both in the negative direction.

Each module has its own power source consisting of a 4S Li-Polymer battery (Figure 3.12), located in the third link (between joints 2 and 3). Control of the servomotors is carried out by the microcontroller (MCU) ESP32, located on the electronic board at the second link (between joints 1 and 2). This board sends and receives information from the servomotors, which have a built-in microcontroller that allows position and velocity control, among others. Dynamixel servomotors communicate via half-duplex UART (TTL daisy chained bus). In this scheme, each motor has a unique ID that allows one-to-one commands to be sent and received through the same shared channel. This greatly simplifies wiring and control. The MCU of the board is also capable of controlling the end effector tool with PWM signals, that is, the suction cup with a turbine that allows the vacuum to be generated. This tool has a pressure and temperature sensor as well as three laser distance transducers that are used to facilitate the alignment of the suction cup with a surface. These suction cup sensors communicate with the MCU via I2C. With feedback from the pressure sensor, it is immediately possible to determine the gripping force achieved by the suction cup, whose design, efficiency and performance are described in more detail in [Hernando et al., 2021b]. The weight and length of the entire module with the suction

cup are 1.94 kg and 711 mm, respectively.

Each module is capable of communicating through multiple means, wireless (Bluetooth -BT-, and Wi-Fi) and wired (CAN bus) with the same protocol. For convenience and being indifferent to the media by which the messages arrive, currently the communication between the modules and the CC is done via Wi-Fi using UDP (User Datagram Protocol) messages. Each module has a unique IP address on the network generated by the router. Communication through BT is used to configure parameters or to obtain operating logs.

The types of messages that can be sent or received are shown in Table 3.5. Simplifying, the MCU sends the status of the module, whereas the CC sends the commands to be executed. The modules are programmed in such a way that when there is a connection to a master device (the CC), they send information about their status at a rate of about 100Hz (main motors variables, suction cup pressure and distance sensors, battery voltage and current consumption). To know that a master is connected, it emits a periodic signal to all modules of the organism. This type of message is known as a heartbeat.

Command	**Data**	**Direction**
Motor info	Id, position, velocity, intensity, temperature, voltage, status	MCU → CC
Module info	Name, network info	
Suction cup info	Pressure, temperature, distance[3]	
Analog info	Battery voltage, current	
Logger	Text	
Motor command	Id, goal position, goal velocity, goal torque, torque (ON/OFF), reboot, control mode, maximum velocity, etc.	CC → MCU
Get module info	None	
Suction cup command	Desired power throttle (%)	
Heartbeat	None	
Change config	Name, network info	

Table 3.5: Main messages between devices.

Lastly, to summarize the behavior of the suction cup and as a result of experiments with the different versions of the suction cups, Figure 3.16 shows the maximum distance between the suction cup and a metal plate to which the suction cup adheres despite focusing on the plate at an angle. The graph shows, for different angles of approach, the critical distance of adhering with different power throttles (%).

3.7 Organism body

According to the premises of ROMERIN, in this dissertation a robotic organism is defined without a predefined structure. The designer is then responsible for ensuring an appropriate arrangement of modules to achieve the desired objectives for a given task. As in the animal world, the unifying element where the legs are attached is called the body and should provide the following components:

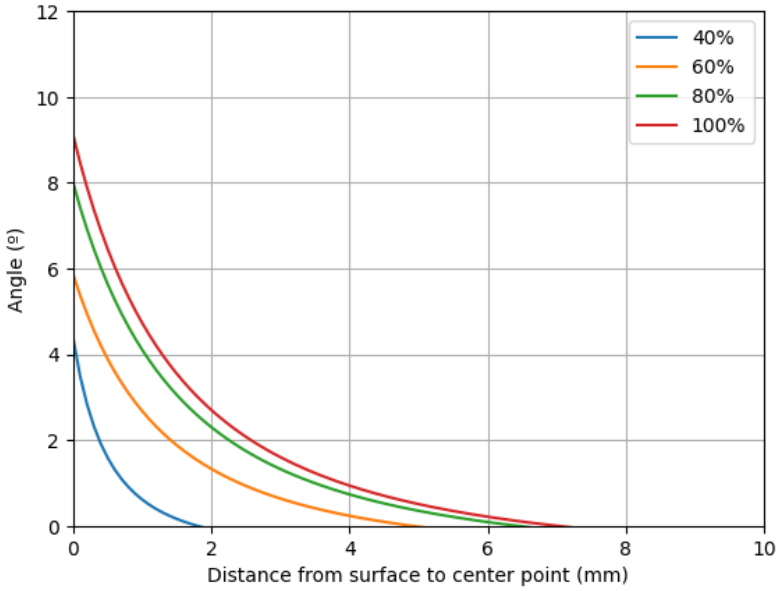

Figure 3.16: Adhesion limits of the suction cup with different power throttles (%).

- A CC: the brain of the organism, responsible for coordination of the robot modules and control of the organism as a whole.
- Reliable physical sockets to attach the modules.
- A wireless router: modules are able to communicate in a variety of ways, so this component is not strictly required, although it is the more flexible and easier way to communicate. Thus, for simplicity, the body currently generates its own Wi-Fi (802.11n) to which the different modules connect. Therefore, there is a specific local network for the whole robot organism.
- A RGBd camera: the main sensor of the robot to perceive the world.
- An accelerometer: mainly used to determine where the gravity vector points.

The body designed in this doctoral thesis and with which we currently validate the concept of the organism and the control strategies is made up of two aluminum plates where the previously detailed components are mounted (Figure 3.17). First of all, we include a "Jetson Xavier NX Developer Kit", 8GB, CPU of 6-core NVIDIA Carmel ARM, 384 NVIDIA CUDA cores, and 48 Tensor cores, as CC. Its small size helps to reduce body volume. Both aluminum plates are custom-made to house four modules, one at each corner of a rectangle with an angle of 45°. The Vonets VAR11N mini router and bridge is used to generate local Wi-Fi, which allows up to 20 devices to be connected. Moreover, we have included the "Depth Camera D435i" of RealSense to perceive the environment, which includes the Bosch BMI055 IMU that is used to determine the gravity direction. It is mounted on a pantilt system moved by two Dynamixel motors "XL330-M2888-T". The control of them is carried out by the CC, which makes use of a "U2D2", a small size USB communication converter that allows one to control and operate Dynamixel motors with a computer. In addition, a DC-DC converter is installed to supply the pantilt system.

Finally, a battery is housed under the bottom plate to supply the CC and the DC-DC converter.

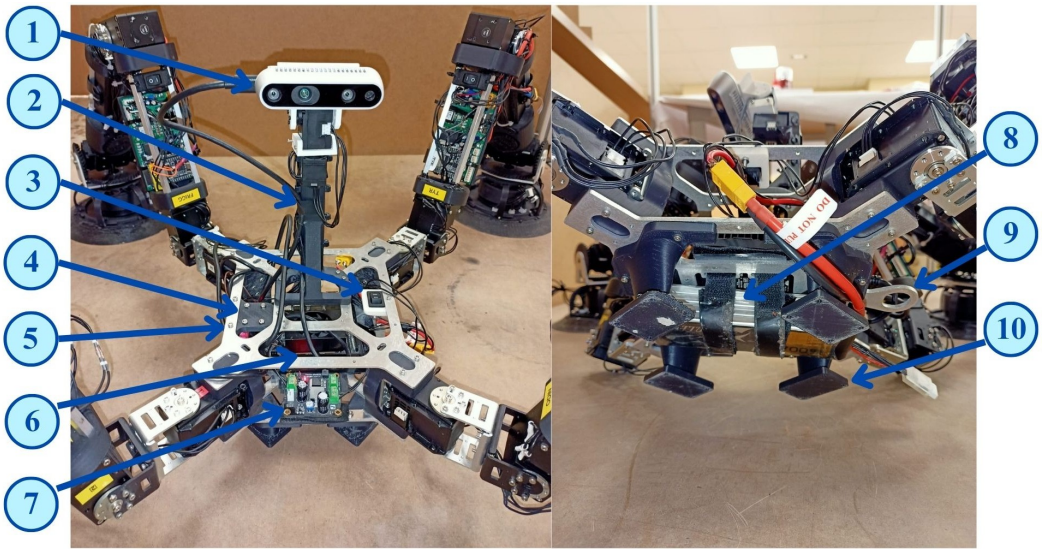

Figure 3.17: Constructed body for a 4-legged robotic organism. (1) RGBd camera, (2) pantilt, (3) switch, (4) IMU, (5) U2D2, (6) CC, (7) DC/DC converter, (8) body battery, (9) safety bracket, and (10) body supporters.

In case of using the embedded IMU of the Realsense D435i camera, it is required to transform the data to the body frame. As shown in Figure 3.17, the camera is located at the top of the body through a pantilt. To obtain gravity on the reference frame of the body Σ_B, the kinematics of the pantilt chain should be obtained (Figure 3.18). Several frames have been obtained to work together with DH parameters (Denavit-Hartenberg) and directly with the transformation matrix. Although displacement is not needed to transform the gravity vector from the camera frame to the base one, they have been included in the table of DH parameters (Table 3.6).

Joint	θ	**d**	**a**	α
1	q_1	L_2	0	$\frac{\pi}{2}$
2	$q_2 + \frac{\pi}{2}$	0	L_3	0

Table 3.6: DH parameters of the pantilt

Then, the transformation of the gravity vector from the camera frame to the robot body frame is as indicated in Equation 3.1:

$$^{B}\vec{g} = {}^{B}T_0 \cdot {}^{0}A_1\left(q_1\right) \cdot {}^{1}A_2\left(q_2\right) \cdot {}^{2}T_C \cdot {}^{C}\vec{g} \tag{3.1}$$

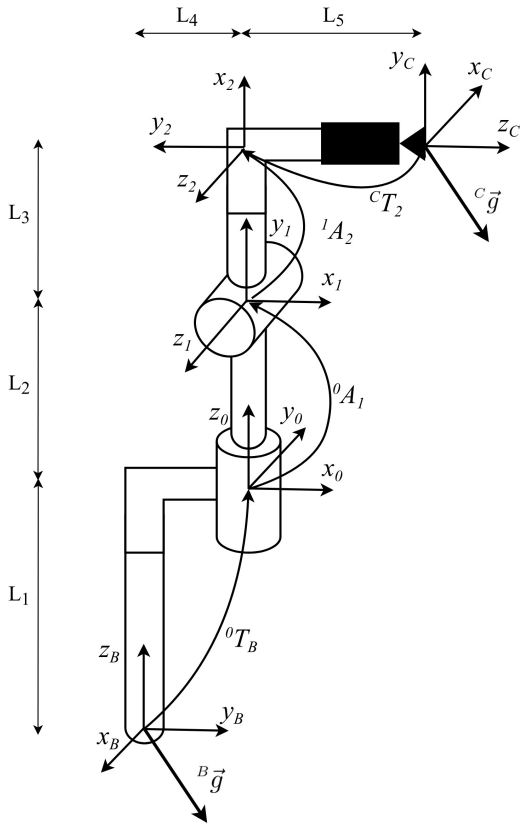

Figure 3.18: Reference frames, dimensions, and transformations of the pantilt.

3.8 Organism configuration and kinematics

3.8.1 Contextualization

The robotic organism is defined as a system composed of N identical modules, where each module $i \in [1, ..., N]$ has J joints and links indicated as $j \in [1, ..., J]$ and $k \in [1, ..., J]$ respectively.

The homogeneous transformation matrix between two reference frames (from $RF1$ to $RF2$) is represented as ${}^{RF1}T_{RF2}$. The following reference frames are defined (Figure 3.19):

- Σ_B is located at the origin of the body (located in the center of mass, COM, by own decision),
- Σ_i is located in the first joint of module i,
- Σ_{iw} is located in the WP of module i,
- Σ_{iS} is located at the contact points (suction cup frame, SC frame) of module i,
- Σ_{ik} is located in the COM of link k of module i,
- $\Sigma_{i,cg}$ is located in the COM of module i,
- Σ_{cg} is located in the COM of the entire robotic organism,

- Σ_C is located in the camera.

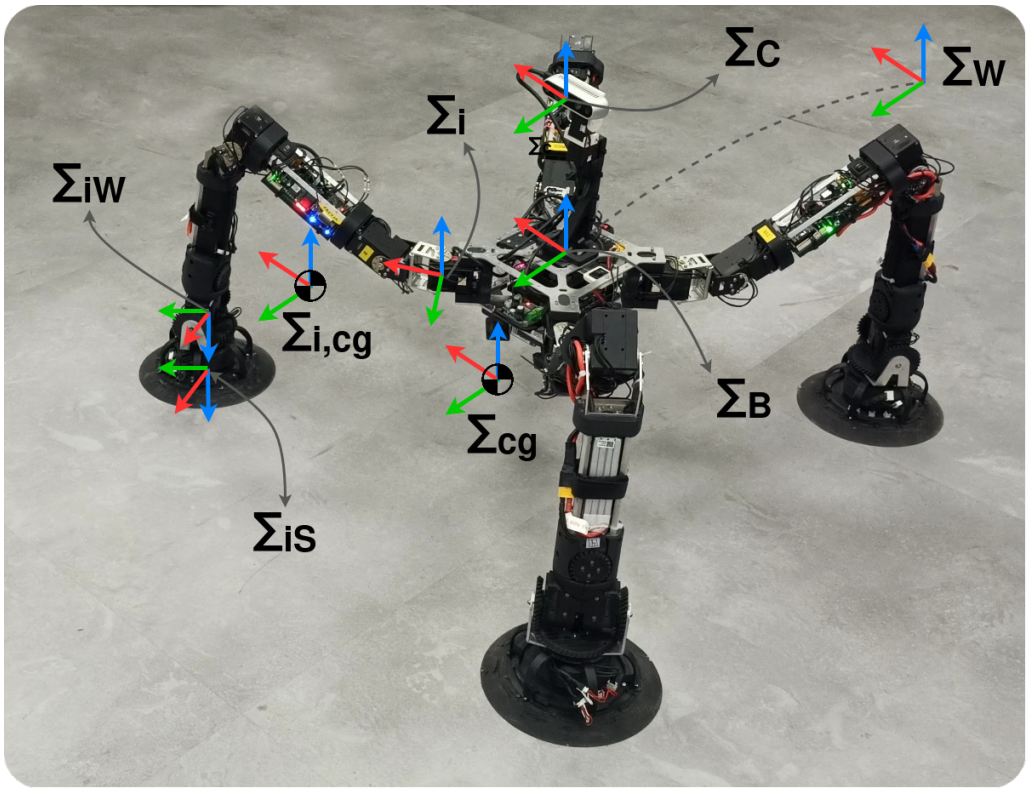

Figure 3.19: Reference frames of the robot.

The following notation is defined for the components mass and dimension:

- m_{ik} represents the mass of the link k of the module i,
- m_i is the total weight of the module i,
- m_B indicates the mass of the body,
- M is the mass of the entire robotic organism,
- L is the maximum length of the module (stretched leg).

Whereas the position of joint j of module i is denoted as q_{ij}, the reaction forces that appear at the wrist point Σ_{iw} due to the interaction of the robot with the environment are represented as $\vec{F}_i$.

3.8.2 Leg kinematics

The kinematic model of each module is shown in Figure 3.20, whose main dimensions and masses are denoted in Table 3.7. The Denavit–Hartenberg (DH) parameters that define the kinematic model are indicated in Table 3.8.

The mathematical model of the kinematic chain is quite complex to obtain analytically, even if the last three joints are removed from the calculations. To reduce the complexity

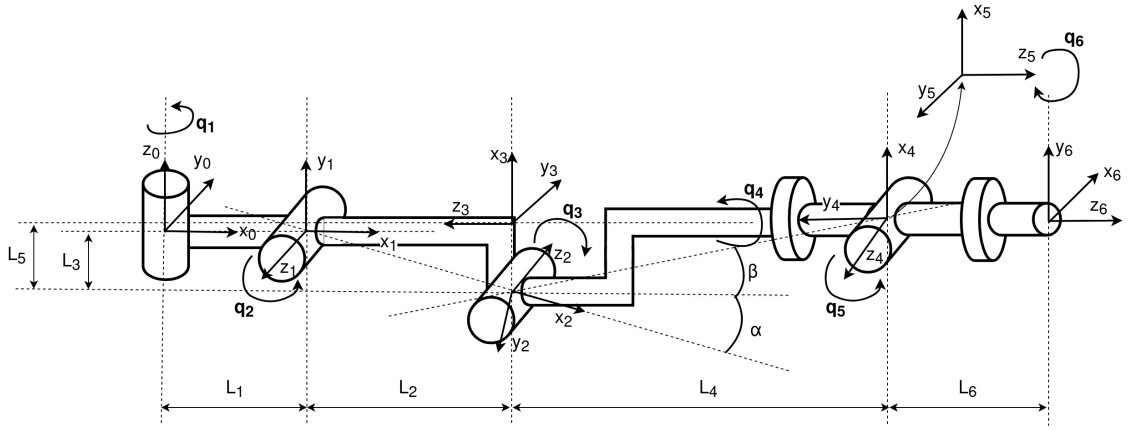

Figure 3.20: ROMERIN module kinematics

Table 3.7: Kinematic model dimensions and links masses.

Name	**Value (m)**	**Name**	**Value (kg)**
L_1	0.068	m_{i1}	0.212
L_2	0.22045	m_{i2}	0.360
L_3	0.01492	m_{i3}	0.535
L_4	0.27991	m_{i4}	0.205
L_5	0.02245	m_{i5}	0.120
L_6	0.087	m_{i6}	0.292
L	0.65536	M	1.724

Table 3.8: DH parameters of the ROMERIN leg module.

Joint	$\boldsymbol{\theta}$	**d**	**a**	$\boldsymbol{\alpha}$
1	q_1	0	L_1	$\frac{\pi}{2}$
2	$q_2 - \alpha$	0	$\frac{L_2}{\cos(\alpha)}$	π
3	$q_3 - \frac{\pi}{2} - \alpha$	0	L_5	$\frac{\pi}{2}$
4	q_4	$-L_3$	0	$\frac{\pi}{2}$
5	q_5	0	0	$\frac{\pi}{2}$
6	$q_6 - \frac{\pi}{2}$	L_6	0	0

of the system, the configuration shown in Figure 3.21 is created, whose DH parameters are indicated in Table 3.9, with the premises that:

$$\alpha = atan(\frac{L_3}{L_2}) = 0.09561 \tag{3.2}$$

$$L_c = \sqrt{L_2^2 + L_3^2} = 0.22095 \tag{3.3}$$

$$\beta = atan(\frac{L_5}{L_4}) = 0.08004 \tag{3.4}$$

$$L_d = \sqrt{L_4^2 + L_5^2} = 0.28081 \tag{3.5}$$

The frame transformation matrices are given as:

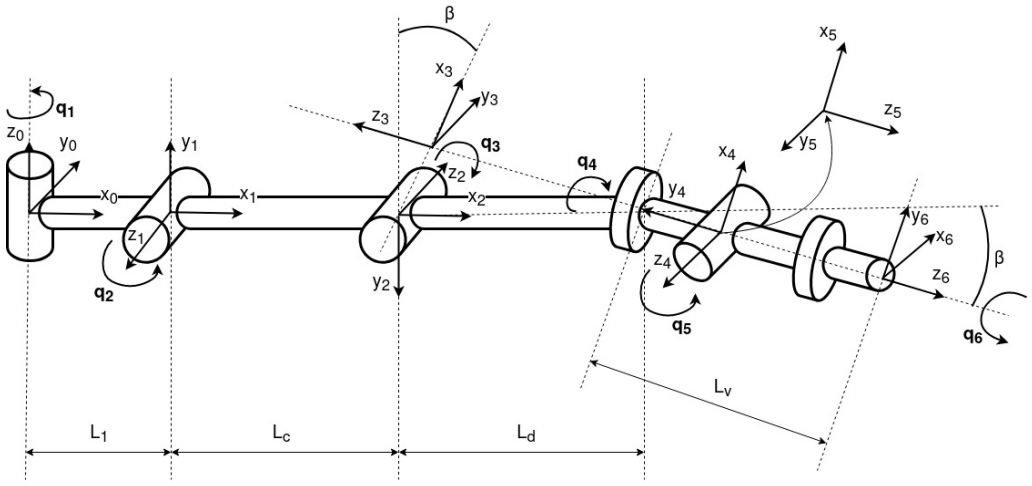

Figure 3.21: ROMERIN module kinematics transforming second and third joints.

Joint	θ	**d**	**a**	α
1	q_1	0	L_1	$\frac{\pi}{2}$
2	q_2	0	L_c	π
3	$q_3 - \frac{\pi}{2} + \beta$	0	$L_d \cdot \sin(\beta)$	$\frac{\pi}{2}$
4	q_4	$-(L_d \cdot cos(\beta))$	0	$\frac{\pi}{2}$
5	q_5	0	0	$\frac{\pi}{2}$
6	$q_6 - \frac{\pi}{2}$	L_S	0	0

Table 3.9: Parts information

$$ {}^{0}A_6 = {}^{0}A_1 \cdot {}^{1}A_2 \cdot {}^{2}A_3 \cdot {}^{3}A_4 \cdot {}^{4}A_5 \cdot {}^{5}A_6 \tag{3.6} $$

$$ {}^{i-1}A_i = \begin{pmatrix} c\theta_i & -c\alpha_i \cdot s\theta_i & s\alpha_i \cdot s\theta_i & a_i \cdot c\theta_i \\ s\theta_i & c\alpha_i \cdot c\theta_i & -s\alpha_i \cdot c\theta_i & a_i \cdot s\theta_i \\ 0 & s\alpha_i & c\alpha_i & d_i \\ 0 & 0 & 0 & 1 \end{pmatrix} \tag{3.7} $$

$$ {}^{0}A_1 = \begin{pmatrix} c_1 & 0 & s_1 & L_1 \cdot c_1 \\ s_1 & 0 & -c_1 & L_1 \cdot s_1 \\ 0 & 1 & 0 & 0 \\ 0 & 0 & 0 & 1 \end{pmatrix} \tag{3.8} $$

$$ {}^{1}A_2 = \begin{pmatrix} c_2 & s_2 & 0 & L_c \cdot c_2 \\ s_2 & -c_2 & 0 & L_c \cdot s_2 \\ 0 & 0 & -1 & 0 \\ 0 & 0 & 0 & 1 \end{pmatrix} \tag{3.9} $$

$$ {}^{2}A_3 = \begin{pmatrix} s_{3+\beta} & 0 & -c_{3+\beta} & L_d \cdot s_\beta \cdot s_{3+\beta} \\ -c_{3+\beta} & 0 & -s_{3+\beta} & -L_d \cdot s_\beta \cdot c_{3+\beta} \\ 0 & 1 & 0 & 0 \\ 0 & 0 & 0 & 1 \end{pmatrix} \tag{3.10} $$

$$ {}^{3}A_4 = \begin{pmatrix} c_4 & 0 & s_4 & 0 \\ s_4 & 0 & -c_4 & 0 \\ 0 & 1 & 0 & -L_d \cdot c_\beta \\ 0 & 0 & 0 & 1 \end{pmatrix} \tag{3.11} $$

$$ {}^{4}A_5 = \begin{pmatrix} c_5 & 0 & s_5 & 0 \\ s_5 & 0 & -c_5 & 0 \\ 0 & 1 & 0 & 0 \\ 0 & 0 & 0 & 1 \end{pmatrix} \tag{3.12} $$

$$ {}^{5}A_6 = \begin{pmatrix} s_6 & c_6 & 0 & 0 \\ -c_6 & s_6 & 0 & 0 \\ 0 & 0 & 1 & L_S \\ 0 & 0 & 0 & 1 \end{pmatrix} \tag{3.13} $$

Multiplying the matrices to obtain ${}^{0}A_6$, the following result is obtained for each component of the rotation matrix:

$$ \begin{aligned} {}^{0}A_6(0,0) = (s_6(c_5(c_4(c_1c_2s_{3+\beta} - c_1s_2c_{3+\beta}) - s_1s_4) + s_5(-c_1c_2c_{3+\beta} - c_1s_2s_{3+\beta})) \\ - c_6(s_4(c_1c_2s_{3+\beta} - c_1s_2c_{3+\beta}) + s_1c_4) \end{aligned} \tag{3.14} $$

$$ \begin{aligned} {}^{0}A_6(0,1) = c_6(c_5(c_4(c_1c_2s_{3+\beta} - c_1s_2c_{3+\beta}) - s_1s_4) + s_5(-c_1c_2c_{3+\beta} - c_1s_2s_{3+\beta})) \\ + s_6(s_4(c_1c_2s_{3+\beta} - c_1s_2c_{3+\beta}) + s_1c_4) \end{aligned} \tag{3.15} $$

$$ {}^{0}A_6(0,2) = s_5(c_4(c_1c_2s_{3+\beta} - c_1s_2c_{3+\beta}) - s_1s_4) - c_5(-c_1c_2c_{3+\beta} - c_1s_2s_{3+\beta}) \tag{3.16} $$

$$ \begin{aligned} {}^{0}A_6(1,0) = s_6(c_5(c_4(s_1c_2s_{3+\beta} - s_1s_2c_{3+\beta}) + c_1s_4) + s_5(s_1(-c_2)c_{3+\beta} - s_1s_2s_{3+\beta})) \\ - c_6(s_4(s_1c_2s_{3+\beta} - s_1s_2c_{3+\beta}) - c_1c_4) \end{aligned} \tag{3.17} $$

$$ \begin{aligned} {}^{0}A_6(1,1) = c_6(c_5(c_4(s_1c_2s_{3+\beta} - s_1s_2c_{3+\beta}) + c_1s_4) + s_5(s_1(-c_2)c_{3+\beta} - s_1s_2s_{3+\beta})) \\ + s_6(s_4(s_1c_2s_{3+\beta} - s_1s_2c_{3+\beta}) - c_1c_4) \end{aligned} \tag{3.18} $$

$$ {}^{0}A_6(1,2) = s_5(c_4(s_1c_2s_{3+\beta} - s_1s_2c_{3+\beta}) + c_1s_4) - c_5(s_1(-c_2)c_{3+\beta} - s_1s_2s_{3+\beta}) \tag{3.19} $$

$$ {}^{0}A_6(2,0) = s_6(c_5c_4(s_2s_{3+\beta} + c_2c_{3+\beta}) + s_5(c_2s_{3+\beta} - s_2c_{3+\beta})) - c_6s_4(s_2s_{3+\beta} + c_2c_{3+\beta}) \tag{3.20} $$

$$ {}^{0}A_6(2,1) = c_6(c_5c_4(s_2s_{3+\beta} + c_2c_{3+\beta}) + s_5(c_2s_{3+\beta} - s_2c_{3+\beta})) + s_6s_4(s_2s_{3+\beta} + c_2c_{3+\beta}) \tag{3.21} $$

$$ {}^{0}A_6(2,2) = s_5c_4(s_2s_{3+\beta} + c_2c_{3+\beta}) - c_5(c_2s_{3+\beta} - s_2c_{3+\beta}) \tag{3.22} $$

Whereas the TCP position (suction cup frame) is given as:

$$\begin{aligned} x_{iS} &= {}^0A_6(0,3) \\ &= L_1c_1 + L_cc_1c_2 - L_dc_1s_2s_\beta c_{3+\beta} + L_dc_1c_2s_\beta s_{3+\beta} - L_dc_\beta(-c_1c_2c_{3+\beta} - c_1s_2s_{3+\beta}) \\ &\quad + L_s(s_5(c_4(c_1c_2s_{3+\beta} - c_1s_2c_{3+\beta}) - s_1s_4) - c_5(-c_1c_2c_{3+\beta} - c_1s_2s_{3+\beta})) \end{aligned} \tag{3.23}$$

$$\begin{aligned} y_{iS} &= {}^0A_6(1,3) \\ &= L_1s_1 + L_cs_1c_2 - L_ds_1s_2s_\beta c_{3+\beta} + L_ds_1c_2s_\beta s_{3+\beta} - L_dc_\beta(s_1(-c_2)c_{3+\beta} - s_1s_2s_{3+\beta}) \\ &\quad + L_s(s_5(c_4(s_1c_2s_{3+\beta} - s_1s_2c_{3+\beta}) + c_1s_4) - c_5(s_1(-c_2)c_{3+\beta} - s_1s_2s_{3+\beta})) \end{aligned} \tag{3.24}$$

$$\begin{aligned} z_{iS} &= {}^0A_6(2,3) \\ &= L_cs_2 + L_ds_2s_\beta s_{3+\beta} + L_dc_2s_\beta c_{3+\beta} - L_dc_\beta(c_2s_{3+\beta} - s_2c_{3+\beta}) \\ &\quad + L_s(s_5c_4(s_2s_{3+\beta} + c_2c_{3+\beta}) - c_5(c_2s_{3+\beta} - s_2c_{3+\beta})) \end{aligned} \tag{3.25}$$

In this first simplified case, the feedback position of the motors should be transformed, as well as the commanded position to each motor. This is, the second joint receives an increment of α, whereas the third joint receives an increment of $\alpha+\beta$ (positive or negative according to the direction, remembering that the second and third joints point oppositely).

To reduce the problems of hyperstaticity, to simplify the kinematic chain, and to be able to compute the reaction forces in the WP, the wrist is disabled when the suction cup is attached to a surface; that is, the last three joints are detached from the power, keeping the feedback from them. To reduce computation complexity, the system can be reduced as shown in Figure 3.22, where the axis z indicates the rotation axis. By doing so, the robot has $(N \cdot 3)$ active DOF without taking into account the first joint, and $(N \cdot 3)$ passive DOF.

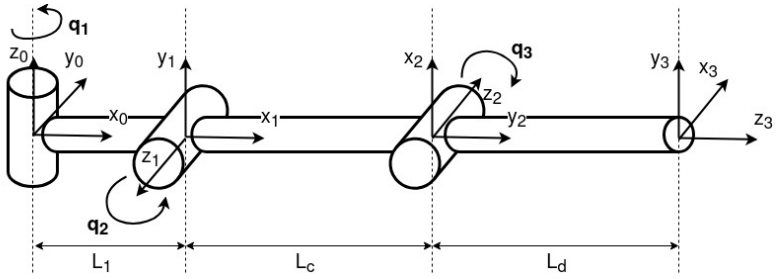

Figure 3.22: ROMERIN module kinematics simplified

In this second case of simplification, the feedback and commanded position of the motors are also transformed. The forward kinematic model of each leg is computed as indicated in Equation 3.26, whose differential is obtained in Equation 3.27.

$$\begin{pmatrix} x_w \\ y_w \\ z_w \end{pmatrix} = \begin{pmatrix} L_1 \cdot c_1 + L_c \cdot c_1 \cdot c_2 + L_d \cdot c_1 \cdot c_{3-2} \\ L_1 \cdot s_1 + L_c \cdot s_1 \cdot c_2 + L_d \cdot s_1 \cdot c_{3-2} \\ L_c \cdot s_2 - L_d \cdot s_{3-2} \end{pmatrix} \tag{3.26}$$

$$\begin{pmatrix} \dot{x}_w \\ \dot{y}_w \\ \dot{z}_w \end{pmatrix} = \underbrace{\begin{pmatrix} -s_1 \cdot (L_1 + L_c \cdot c_2 + L_d \cdot c_{3-2}) & -L_c \cdot c_1 \cdot s_2 + L_d \cdot c_1 \cdot s_{3-2} & -L_d \cdot c_1 \cdot s_{3-2} \\ c_1 \cdot (L_1 + L_c \cdot c_2 + L_d \cdot c_{3-2}) & -L_c \cdot s_1 \cdot s_2 + L_d \cdot s_1 \cdot s_{3-2} & -L_d \cdot s_1 \cdot s_{3-2} \\ 0 & L_c \cdot c_2 + L_d \cdot c_{3-2} & -L_d \cdot c_{3-2} \end{pmatrix}}_{J(q)} \cdot \begin{pmatrix} \dot{q}_1 \\ \dot{q}_2 \\ \dot{q}_3 \end{pmatrix} \tag{3.27}$$

In this case, inverse kinematics is obtained by:

$$q_1 = atan2(y_w, x_w) \tag{3.28}$$

$$q_3 = \arccos\left(\frac{\left(\frac{x_w}{c_1} - L_1\right)^2 + z_w^2 - L_c^2 - L_d^2}{2 \cdot L_c \cdot L_d}\right) \tag{3.29}$$

$$q_2 = \arctan 2\left(z_w, \left(\frac{x_w}{c_1} - L_1\right)\right) + \arctan 2\left(L_d \cdot s_2, L_c + L_d \cdot c_2\right) \tag{3.30}$$

Although the calculation of q_3 should be considered in two ways, positive and negative, only positive values are considered to avoid that the elbow goes under the body.

3.9 Summary

ROMERIN is a modular legged robot with climbing capabilities using custom-made active suction cups. This doctoral thesis makes use of several modular legs designed initially before the start of the thesis. Due to requirements of legs improvement, the three main versions of the leg modules are described. The first includes the initial design of the legs, whereas the second and third ones include the modifications carried out in collaboration with other students.

This chapter also includes how leg modules communicates with the central controller (CC), the main messages that both components interchange, and a description of the main components of the organism body.

Lastly, it gives a contextualization of the organism configuration and kinematics, describing the different reference frames of the organism. It includes a deep description of the leg kinematics, and a simplification by transforming the second and third joints that facilitates the analytical calculation of the kinematic chain. It finally includes a simplification of the kinematics by removing the wrist actuators and suction cup. This simplification is useful to reduce the problem of hyperstaticity and to enable the computation of the reaction forces in the WP. The different kinematic chains have been used depending on the leg state according to explained in Section 4.1.3.

The content included in this chapter has been partially published in [Hernando et al., 2022].